Thermocapillary Convection in a Model Float Zone

J. R. Hyer,* D. F. Jankowski,† and G. P. Neitzel‡
Arizona State University, Tempe, Arizona 85287

A finite element method has been used to study thermocapillary convection in a model of relevance to the float-zone, crystal-growth process. The geometry consists of a pair of horizontal isothermal surfaces with a Boussinesq liquid suspended between them. Because of the variation of surface tension with temperature, the temperature gradient along the free surface drives thermocapillary convection. The free surface is allowed to deform, and its location is calculated along with the velocity and temperature fields. Cases in which thermocapillarity dominates and others in which it interacts with an unstable axial buoyancy gradient are treated. To obtain information of possible interest to potential microgravity applications, the influence of the Grashof number is investigated.

Introduction

THE field of solid-state electronics would benefit by improved methods for growing high-quality crystals of various kinds. In view of the significance of macroscopic heat and mass transport in crystal-growth processes, it is clear that fluid mechanics plays an important role in their manufacture. Indeed, there is a significant literature (e.g., the review article by Ostrach[1]) on various fluid-mechanical aspects of these processes.

The float-zone process is an attractive way to produce high-quality single crystals because the absence of solid restraining walls significantly reduces contamination by impurities. In this process, a rod of polycrystalline material is pulled slowly through a heating device that melts a portion of the rod; upon resolidification, a single crystal is (hopefully) produced. A drawback is that the molten zone must be small enough to be contained by surface-tension forces. The hope that larger crystals might be manufactured outside the constraints imposed by the Earth's gravitational field, coupled with the unique opportunity provided by the Space Shuttle, has attracted considerable attention to the possibility of using this technique in a microgravity environment.

Although the float-zone process is not completely understood, several theoretical and experimental models of the pertinent fluid mechanics have been created to study various aspects of the mechanisms involved. While buoyancy forces will be significantly reduced in a microgravity environment, another mode of convection will persist. This is driven by the temperature dependence of surface tension coupled with temperature differences along a free surface and is known as thermocapillary convection. One important model that isolates the effect of thermocapillary convection is the so-called half zone, which models the bottom half of an actual float zone. Experiments[2-4] performed for such half zones have shown that thermocapillary convection can become unstable, undergoing a transition to oscillatory convection. These oscillations, when coupled with the solidification process in a real float zone, are believed to be responsible for the existence of undesirable striations in the material. The theoretical investigation of this instability is the underlying motivation for the present work. Such an analysis will be useful in bridging the gap in Prandtl number between real semiconductor materials [$Pr = \mathcal{O}(10^{-2})$] and fluids used in model experiments [$Pr = \mathcal{O}(10)$].

The first step in a stability analysis is the determination of an appropriate basic state, i.e., the velocity, pressure, and temperature fields that are a solution to the governing equations. Shen et al.,[5] Fu and Ostrach,[6] and Kobayashi[7] have obtained numerical solutions for half and full zones with nondeformable free surfaces. However, an actual zone exhibits free-surface deformation due to a combination of body force and convective effects. The major purpose of the present computations is to provide a half-zone basic state for a subsequent stability analysis that includes this effect. The anticipated irregular geometry suggests the use of a finite element method. Such ideas have been successfully employed in a similar plane problem by Cuvelier and Driessen.[8] Since a full zone requires only minor changes in boundary conditions and provides a means for studying the interaction between thermocapillarity and a potentially unstable axial buoyancy gradient, some results for this case are also included.

The mathematical models will be discussed in the next section, followed by a description of the application of finite element concepts. Finally, results and conclusions will be presented.

Mathematical Model

The assumptions that form the basis for the mathematical model of the half zone are the following.

1) The flow domain consists of a liquid bounded by upper and lower solid, planar, circular surfaces and an unknown free surface.

2) For the half zone, the upper surface is maintained at a temperature T_H that is greater than the T_C of the lower surface; for the full zone, both surfaces are maintained at T_C.

3) Only convective heat transfer at the free surface is considered. (This is to preserve the quadratic nature of the energy functional[5] in the initial stability analysis. It will be relaxed in a subsequent analysis.)

4) The velocity and temperature fields and the free-surface deformation are axisymmetric with the axis of symmetry of the zone taken to be parallel to the direction of gravity.

5) The Boussinesq approximation is made and surface tension is assumed to vary linearly with temperature.

The solution domain, coordinate system, and associated physical dimensions for the half zone are shown in Fig. 1. With these assumptions, the solution domain can be treated as

Received Jan. 2, 1990; presented as Paper 90-0406 at the AIAA 28th Aerospace Sciences Meeting, Reno, NV, Jan. 9-12, 1990; revision received April 17, 1990; accepted for publication April 20, 1990.

*Graduate Research Assistant, Department of Mechanical and Aerospace Engineering.

†Professor, Department of Mechanical and Aerospace Engineering. Member AIAA.

‡Professor, Department of Mechanical Engineering; currently Professor, George W. Woodruff School of Mechanical Engineering, Georgia Institute of Technology, Atlanta, GA. Associate Fellow AIAA.

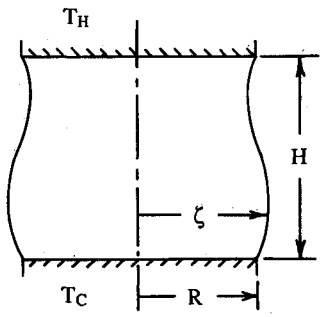

Fig. 1 Half-zone definition sketch.

if it were two dimensional. The governing balance equations for mass, momentum, and energy, in dimensionless form, are

$$A(ru)_r + (rw)_z = 0 \tag{1}$$

$$Auu_r + wu_z = -Ap_r + Re^{-1}[Ar^{-1}(ru_r)_r + A^{-1}u_{zz} - Au/r^2] \tag{2}$$

$$Auw_r + ww_z = -p_z + (A\,Gr/Re^2)T + Re^{-1}[Ar^{-1}(rw_r)_r + A^{-1}w_{zz}] \tag{3}$$

$$AuT_r + wT_z = Ma^{-1}[Ar^{-1}(rT_r)_r + A^{-1}T_{zz}] \tag{4}$$

Here, u and w are the radial and axial velocity components scaled by a thermocapillary velocity:

$$u^* = \gamma\Delta T/\mu$$

where γ is the constant rate of change of surface tension with temperature, μ is the coefficient viscosity, and $\Delta T = T_H - T_C$ is the appropriate temperature difference; for the full zone, T_H is everywhere replaced by $T_a(L/2)$, where the temperature $T_a(z)$ is the specified temperature of the assumed surrounding passive gas.

The radial and axial coordinates r and z have been scaled by the radius R and zone height L, respectively, which leads to the appearance of the aspect ratio $A = L/R$. The nondimensionalized pressure is

$$p = (p^* + \rho_0 gLz)/\rho_0 u^{*2}$$

where p^* is the dimensional pressure, g is the gravitational acceleration, and ρ_0 is the density corresponding to the mean temperature $T_0 = (T_H + T_C)/2$. The dimensionless temperature is

$$T = (T^* - T_0)/\Delta T$$

where T^* is the dimensional temperature.

The boundary conditions of no slip, no penetration, and temperature continuity at the endwalls require

$$u = w = 0 \quad \text{at} \quad z = 0, 1 \tag{5a–d}$$

$$T = -1/2 \quad \text{at} \quad z = 0 \tag{6a}$$

$$\text{half zone} \qquad T = 1/2 \quad \text{at} \quad z = 1 \tag{6b}$$

$$\text{full zone} \qquad T = -1/2 \quad \text{at} \quad z = 1 \tag{6c}$$

Symmetry conditions at the centerline of the zone are

$$u = w_r = T_r = 0 \quad \text{at} \quad r = 0 \tag{7a–c}$$

On the free surface, the flow must satisfy the following normal- and shear-stress balances, a heat transfer balance, and the usual kinematic boundary condition.

Normal stress balance:

$$-p + Fr^{-1}z + 2A\,Re^{-1}K^{-2}[Au_r - A^{-1}\zeta_z(u_z + Aw_r) + A^{-2}\zeta_z^2 w_z] = -Re^{-1}(Ca^{-1} - T)[A(\zeta K)^{-1} - A\zeta_{zz}K^{-3}] \tag{8}$$

Shear-stress balance:

$$K^{-1}[2\zeta_z(Au_r - w_z) + A^{-1}(A^2 - \zeta_z^2)(u_z + Aw_z)] = -(\zeta_z T_r + T_z) \tag{9}$$

Heat transfer balance:

$$T_r - A^{-2}\zeta_z T_z = -KA^{-1}Bi[T - T_a(z)] \tag{10}$$

Kinematic boundary condition:

$$u = A^{-1}w\zeta_z \tag{11}$$

where Eqs. (8–11) are applied at the location $r = \zeta$ of the free surface, and $T_a(z)$ is now the nondimensional passive-gas temperature.

The preceding conditions are insufficient to specify the position of the free surface. Possible conditions at the contact line are fixed contact angles or fixed contact points (a so-called "pinning" condition). The latter, which are a more natural choice[9] for the problem of interest, were used, i.e.,

$$\zeta = 1 \quad \text{at} \quad z = 0, 1 \tag{12a,b}$$

Finally, a condition is needed to ensure that the liquid volume is conserved, namely,

$$\int_0^1 \zeta^2\,dz = \text{const} \tag{13}$$

The scaling process has resulted in the appearance of several dimensionless parameters in the equations and boundary conditions. In addition to the aspect ratio, which has already been defined, we have the following.

Reynolds number:

$$Re = u^*R/\nu$$

Capillary number:

$$Ca = \gamma\Delta T/\sigma_0$$

Grashof number:

$$Gr = \beta g\Delta TR^3/\nu^2$$

Marangoni number:

$$Ma = u^*R/\alpha$$

Froude number:

$$Fr = u^{*2}/gL$$

Biot number:

$$Bi = hR/k$$

and, finally, a parameter related to the geometry of the deformed surface,

$$K = (A^2 + \zeta_z^2)^{-1/2}$$

The dimensional quantities appearing in these parameters that have not yet been defined are the kinematic viscosity ν, the mean surface tension σ_0, the coefficient of volumetric expansion β, the thermal diffusivity α, the heat transfer coefficient h, and the thermal conductivity k. The Prandtl number $Pr = \nu/\alpha$ does not appear explicitly in these equations but may be recovered as the ratio Ma/Re.

Finite Element Solution

Except for the complications introduced by the existence of an unknown free boundary, the mathematical problem described in the previous section is readily solved by either a finite element or finite difference[5,6] method. It is possible to formulate a numerical problem so that the free surface position is determined simultaneously with the velocity, pressure, and temperature fields.[8,10] An alternate approach, also used by Cuvelier and Driessen, which was adopted here, relaxes the normal-stress boundary condition, Eq. (8), assumes an initial free-surface position, and then determines the corresponding fields. Iteration is employed by integrating the condition in Eq. (8) to determine a new ζ, and the process is repeated to convergence. Further discussion on this feature of the computation is provided later.

The Galerkin finite element method is employed in a standard way to replace the partial-differential equations, Eqs. (1–4), by their weak forms. A weak form of the normal-stress boundary condition of Eq. (8) is also obtained. In the usual way, mixed interpolation is used, i.e., the variables u, w, and T are approximated on eight-noded elements using quadratic interpolation, and p is approximated on four-noded elements with linear interpolation. The deformable grid is chosen so that the z position of each node is held constant, while the r position moves radially by an amount that is proportional to the position of the free surface. A typical deformed uniform mesh is shown in Fig. 2

From employing interpolation over each element, summing over all elements, and imposing the essential boundary conditions, a set of nonlinear algebraic equations results. The unknowns are the nodal values of u, w, T, and p. This system is solved by Newton iteration. At each iteration, the corresponding linear system is solved by a technique that exploits the banded structure of the Jacobian matrix that arises from a global node ordering. This inner procedure yields a solution for a given free surface. The initial free surface is obtained by determining the free-surface solution corresponding to a static zone under isothermal conditions. The volume of liquid in the zone was arbitrarily chosen to be equal to unity, corresponding to the dimensionless volume of a right circular cylinder of unit radius and height. Subsequent outer iterations adjust the free-surface position to satisfy the normal-stress balance, Eq. (8).

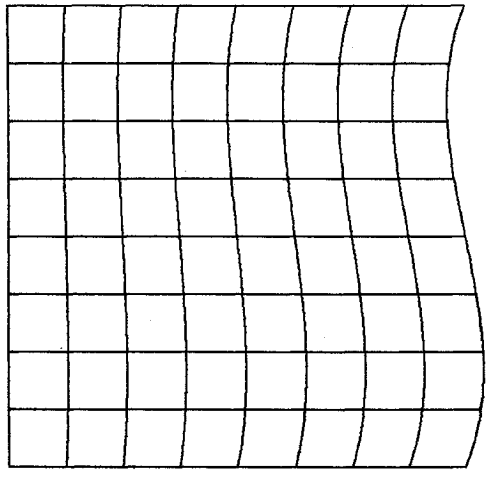

Fig. 2 Deformed mesh.

To compute solutions in various regions of parameter space, solutions for nearby values of parameters were used as initial guesses. This accelerates the convergence process. Experience indicates the code to be fairly robust in its ability to obtain converged solutions for a reasonable variety of parameters. A relative convergence criterion of 10^{-3} for the free surface and 10^{-5} for primitive variables typically requires 4–5 inner iterations to compute the flow for a given free surface; 4–5 outer iterations were usually sufficient for convergence of the free-surface position.

Results and Discussion

Before computing states of thermocapillary convection with free-surface deformation, the inner-iteration portion of the code was verified by comparisons with finite difference calculations for a nondeformable free surface[5] with favorable results. A verification of the outer iteration for the deformed free surface was done for the simplified case of an isothermal half zone and the results are compared with some experimental results[11] for $NaNO_3$ in Fig. 3. The figure shows the calculated free-surface shape along with a photograph of the actual half zone, and the agreement is quite satisfactory, given the nonideal conditions of the experiment. Since the zone is assumed to be isothermal, the numerical solution results in a state of rest, with deformation due only to gravitational effects. In the experimental case, however, although the cylindrical ends are maintained at equal, nearly uniform temperatures, there will undoubtedly be temperature variations within the zone and on the free surface due to convective, conductive, and radiative heat transfer at the free surface itself. These will drive both thermocapillary and buoyant convection. However, no vigorous convection within the zone was observed during the course of the experiments, and so the comparison with the computation may be a fair one. The excellent agreement between calculated and actual free-surface shapes provides some confidence that numerical solutions to be obtained for dynamic cases may be faithful to what would be observed in the laboratory.

Subsequent to these test cases, computations were performed for thermocapillary convection in sodium nitrate half zones corresponding to terrestrial and microgravity body-force levels. Full-zone calculations for Si were also done. A list of parameter values for these computations can be found in Table 1. The dimensionless parameters selected were based upon a given radius (3 mm for the half zone, 2 mm for the full zone). The selection for the half zone was motivated by the model experiments[2]; the full-zone value was selected arbitrarily. The dimensional temperature difference was increased in increments, in accordance with the procedure for changing parameters in the experiments, thereby providing cases that may be more meaningful than those obtained by varying the parameters arbitrarily. For the full-zone cases, heating is provided through a parabolic environment temperature $T_a(z)$, coupled with a nonzero value of the Biot number.

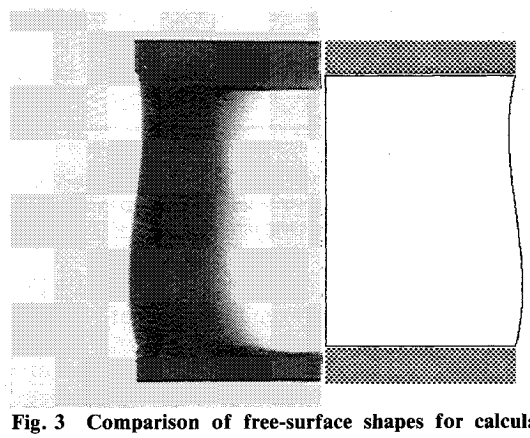

Fig. 3 Comparison of free-surface shapes for calculated and experimental isothermal zones.

Table 1 Parameter values for half- and full-zone computations for $NaNO_3$ and Si

Type	*Pr*	ΔT, °C	*A*	*Re*	*Ca*, × 10^3	*Fr*	*Gr*	*Bi*	*g*, m/s^2
half	7	0.5	1.50	20	0.23	0.002	23	0	9.8
half	7	2.5	1.50	99	1.1	0.054	115	0	9.8
half	7	5.0	1.50	198	2.3	0.217	229	0	9.8
half	7	7.5	1.50	297	3.4	0.489	344	0	9.8
half	7	10.0	1.50	396	4.6	0.870	459	0	9.8
half	7	12.5	1.50	496	5.7	1.36	574	0	9.8
half	7	15.0	1.50	595	6.9	1.96	688	0	9.8
half	7	0.5	1.50	20	0.23	212	2.35×10^{-4}	0	10^{-4}
half	7	2.5	1.50	99	1.1	5×10^3	1.17×10^{-3}	0	10^{-4}
half	7	5.0	1.50	198	2.3	2×10^4	2.34×10^{-3}	0	10^{-4}
half	7	7.5	1.50	297	3.4	5×10^4	3.51×10^{-3}	0	10^{-4}
half	7	10.0	1.50	396	4.6	9×10^4	4.68×10^{-3}	0	10^{-4}
half	7	10.0	1.37	396	4.6	0.870	459	0.5	9.8
half	7	10.0	1.37	396	4.6	0.870	459	2.0	9.8
full	0.023	0.05	2.00	139	0.3	0.015	5	100	9.8
full	0.023	0.25	2.00	694	1.5	0.381	25	100	9.8
full	0.023	0.50	2.00	1388	3.0	1.52	51	100	9.8
full	0.023	0.75	2.00	2082	4.5	3.43	76	100	9.8
full	0.023	1.00	2.00	2777	6.0	6.09	101	100	9.8

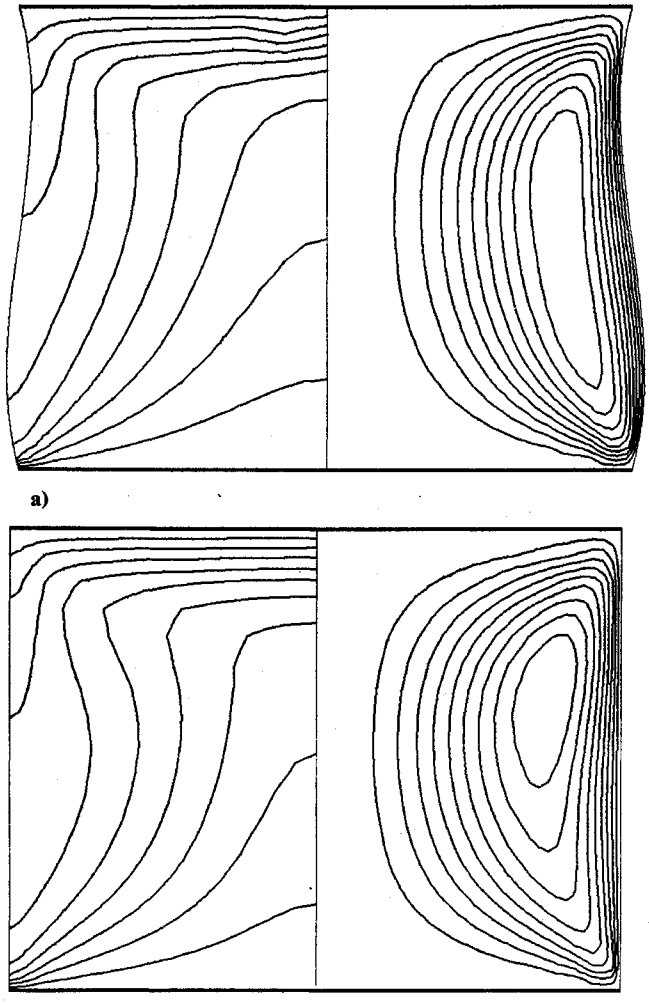

Fig. 4 Isotherms and lines of constant meridional stream function for a half zone of $NaNO_3$ under a) terrestrial and b) microgravity conditions. For both cases, ΔT = 5°C, corresponding to *Re* = 198 (*Ma* = 1386).

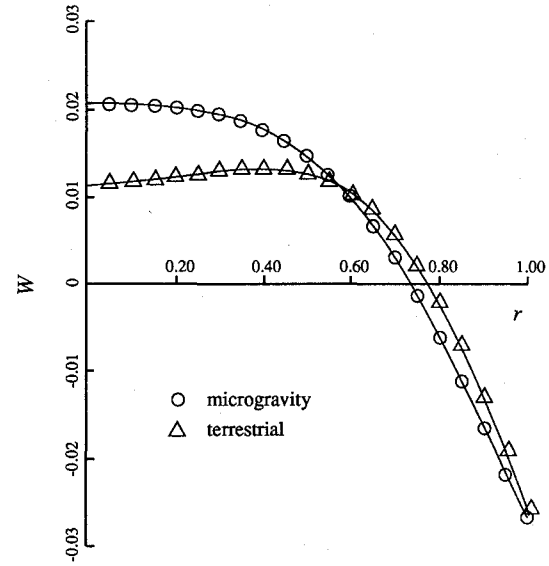

Fig. 5 Radial profiles of the axial velocity within half zones subject to terrestrial and microgravity conditions. Parameters are the same as for Fig. 4.

Figure 4 shows a comparison between half zones of $NaNO_3$ calculated for terrestrial (Fig. 4a) and microgravity (Fig. 4b) body-force levels. Both cases exhibit substantial distortion of the isotherms from a horizontal, pure conduction pattern due to the combination of Reynolds and Prandtl numbers. Those for the microgravity case are more distorted, especially in the upper portion of the half zone, than those calculated under terrestrial conditions. The free-surface deformation experienced by the zone in a microgravity environment is not visible on the scale of the drawing (it is less than 0.5%), whereas the deformation calculated for the terrestrial environment is comparable to that seen in the static case. In fact, for all cases considered, little flow-induced deformation was observed. The other noticeable difference in the two patterns is in the shape of the thermocapillary eddy, the eddy for the microgravity case having a more oval, less elongated appearance than that for the terrestrial case.

The differences between the terrestrial and microgravity cases may also be seen by examining the velocity profiles within the zone. For the same cases presented in Fig. 4, Fig. 5 shows the axial velocity *w* as a function of radius at the half height of the zone. The effect of buoyancy is to retard the return flow near the centerline of fluid that was originally adjacent to the lower, cold wall.

As noted in Table 1, limited calculations were performed for nonzero values of *Bi* to investigate the effect of convective heat transfer at the free surface. For *Bi* = 0.5, the isotherm pattern is only slightly distorted from the pattern for the insulated free surface. For *Bi* = 2, however, significant changes are observed. These calculations have assumed that *Bi* is con-

stant, which is probably unlikely. However, at the present time there is no rational basis for a more complex choice. In particular, it is not known precisely what *Bi* should be to model the thermal environment of a specific experiment.

There is one problem that was encountered in the solution of terrestrial cases (for which a background hydrostatic pressure exists) that is worthy of note. To determine the pressure uniquely within the zone, some sort of "normalization" criterion needs to be selected. Commonly, the pressure is arbitrarily set to some value at one of the computational nodes. At this pressure-specification point, round-off error can accumulate, resulting in the appearance of an artificial "sink" at that location. The impact of this sink can be minimized through a judicious choice for the location of the pressure-specification point. For the calculations presented in this paper, this point was fixed in the upper-left quadrant of the mesh, i.e., near the centerline/hot-wall intersection. When mesh refinement was used, this was done near the free surface and the cold wall, and so this choice for the pressure-specification point places it far away from a region of refined mesh, as recommended by Jackson.[12] In spite of these efforts, the problem is not completely eliminated. Its effect becomes more prominent as the Reynolds number increases, as may be seen in Fig. 6.

One other comparison is possible between the present half-zone calculations and the experiments of Preisser et al.,[2] for which measurements of the axial velocity along the free surface were reported. In Fig. 7, these are shown along with results in dimensional form from the numerical simulation. Since the free-surface velocity is a function of the local driving force, and this varies along the free surface due to the surface-temperature gradient, the surface speed is a function of axial position. The data presented from Preisser et al.[2] are for zones with L = 2.2 mm and 4.1 mm. If one extrapolates the experimental results to the condition $\Delta T = 0$, a nonzero speed is obtained. This is indicative of the nonideal conditions of the experiment and the influence of free-surface heat transfer. The numerical results display a slight bump near $\Delta T = 5°C$, caused by mesh refinement necessary as ΔT, and hence *Re*, increases.

The surface-temperature gradient mentioned before in connection with the driving force is also important in considerations of flow stability. Surface-temperature profiles for several half-zone cases are shown in Fig. 8. The profile is seen to become flatter in the middle of the zone as *Re* increases, with the overall profile taking on an S-shaped appearance. Ostrach[1] has postulated an instability mechanism for thermocapillary convection based on this property. For the highest Reynolds number shown here, corresponding to *Ma* = 2772, the profile is approaching one for which stability considerations are becoming important.

Full-zone computations were performed for several terrestrial cases, which are more interesting than their microgravity counterparts because of the interaction between thermocapillary convection and a potentially unstable buoyancy gradient in the upper half of the zone. The reader is reminded that the heat transfer that drives all convection in this case is provided through the assumption of a parabolic environment temperature, coupled with a nonzero choice for the Biot number. For low Reynolds numbers, the flow is dominated by thermocapillarity, as seen in the degree of midplane symmetry of the flow in Fig. 9a; as the Reynolds number is increased significantly (Fig. 9b), the buoyancy gradient in the upper half of the zone drives convection that reinforces the motion due to thermocapillarity, causing the upper cell to grow in size at the expense of the lower.

The environment of an actual float zone is far more complex than that of the present full-zone model problem. Most notably, the existence of unknown melting and freezing interfaces and counter-rotation of the feed/seed rods complicates the picture presented here. In particular, the latter drives a forced convection, in addition to the thermocapillary and buoyant convection that already exists.

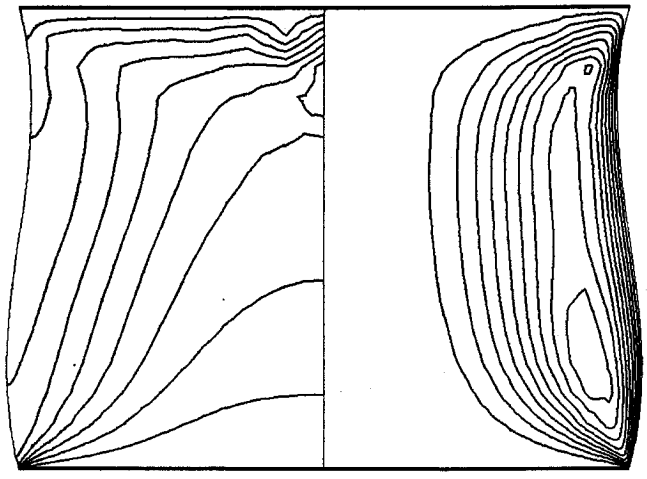

Fig. 6 Isotherms for a half zone of $NaNO_3$ under terrestrial conditions for *Re* = 595 (*Ma* = 4165) showing distortion near the pressure-specification point.

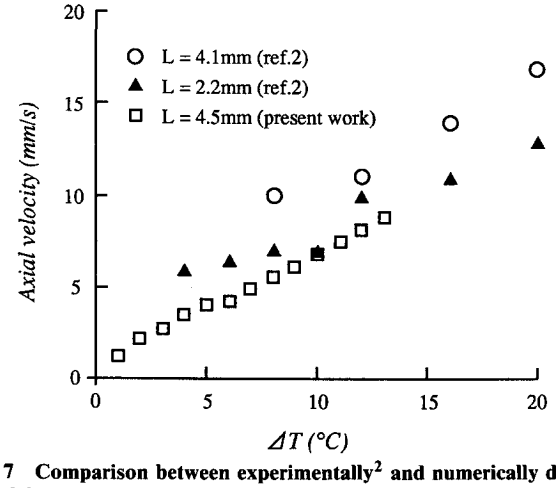

Fig. 7 Comparison between experimentally[2] and numerically determined free-surface axial speeds.

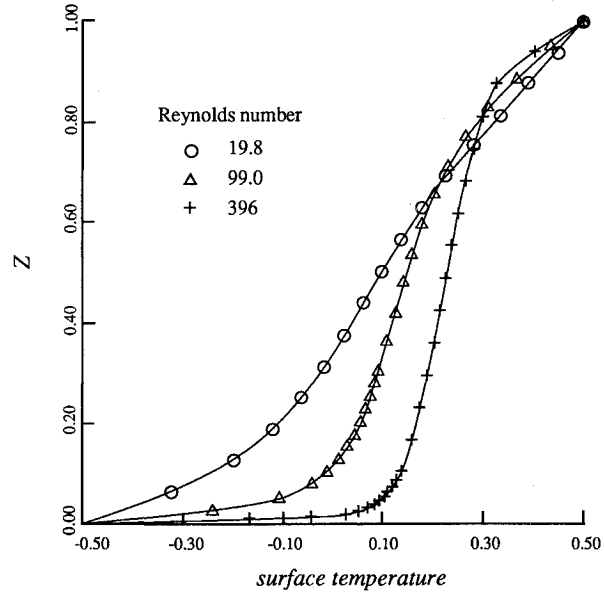

Fig. 8 Surface-temperature profiles for half zones of $NaNO_3$ for various Reynolds numbers.

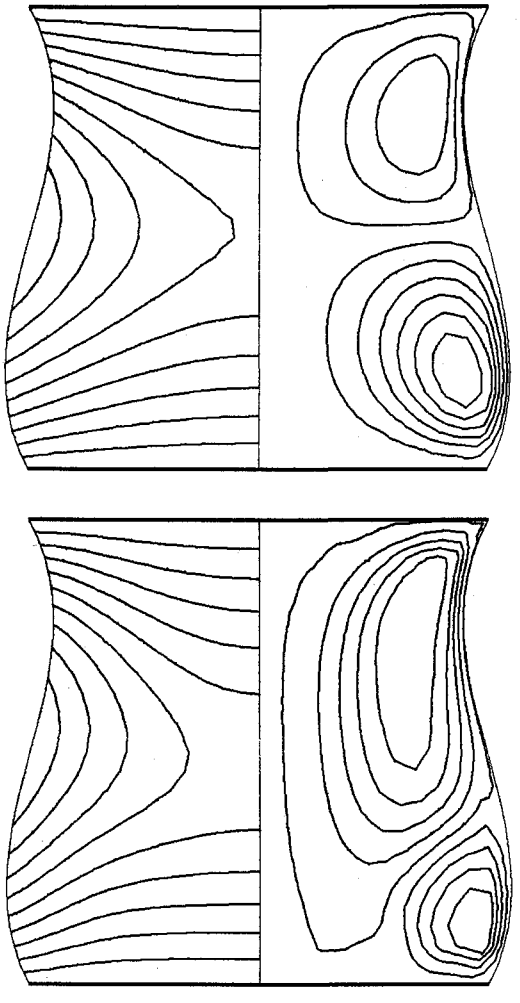

Fig. 9 Full-zone solutions for Si in a terrestrial environment: a) *Re* = 139 (*Ma* = 3.20); b) *Re* = 2082 (*Ma* = 47.89).

In spite of the simplifying assumptions employed in the present analysis, the finite element code that has been developed is capable of determining solutions for the flow and thermal environments within model half and full zones that have a relationship to the float-zone crystal-growth process. The calculation of states with a deformable free surface, both in terrestrial and microgravity environments, shows that there is little flow-induced deformation of the free surface, even at moderate Reynolds numbers. At higher values of the Reynolds number, some difficulties were encountered that were associated with the pressure-specification point. Clearly, mesh refinement is not the answer to this problem. It is speculated that the implementation of a penalty finite element method may be successful in this regard, and this is being pursued. The computer code is capable of obtaining solutions over a wide range of the governing parameters of the problem, in particular, for cases of interest in determining the stability properties of such flows. It should, therefore, be possible to calculate relevant basic states for such subsequent stability analyses.

Acknowledgments

This work was sponsored by the Microgravity Science and Applications Division of NASA. We are indebted to Dietrich Schwabe for kindly performing isothermal half-zone experiments that were used to assist in verification of the code.

References

[1]Ostrach, S., "Fluid Mechanics in Crystal Growth—The 1982 Freeman Scholar Lecture," *ASME Journal of Fluids Engineering,* Vol. 105, 1983, pp. 5–20.

[2]Preisser, F., Schwabe, D., and Scharmann, A., "Steady and Oscillatory Thermocapillary Convection in Liquid Columns with Free Cylindrical Surface," *Journal of Fluid Mechanics,* Vol. 126, 1983, pp. 545–567.

[3]Chun, C.-H., "Verification of the Oscillatory State of Thermocapillary Convection in a Floating Zone under Low Gravity," *Acta Astronautica,* Vol. 7, 1980, pp. 479–488.

[4]Kamotani, Y., Ostrach, S., and Vargas, M., "Oscillatory Thermocapillary Convection in a Simulated Float-Zone Configuration," *Journal of Crystal Growth,* Vol. 66, 1984, pp. 83–90.

[5]Shen, Y., Neitzel, G. P., Jankowski, D. F., and Mittelmann, H. D., "Energy Stability of Thermocapillary Convection in a Model of the Float-Zone, Crystal-Growth Process," *Journal of Fluid Mechanics,* Vol. 217, 1990, pp. 639–660.

[6]Fu, B.-I., and Ostrach, S., "Numerical Solutions of Thermocapillary Flows in Floating Zones," *Transport Phenomena in Materials Processing,* American Society of Mechanical Engineers PED, New York, Vol. 10, HTD, Vol. 29, 1983, pp. 1–9.

[7]Kobayashi, N., "Steady Convection Caused by the Temperature Inhomogeneity in a Cylindrical Floating Zone," *Japanese Journal of Applied Physics,* Vol. 27, 1988, pp. 20–24.

[8]Cuvelier, C., and Dreissen, J. M., "Thermocapillary Free Boundaries in Crystal Growth," *Journal of Fluid Mechanics,* Vol. 169, 1986, pp. 1–26.

[9]Sen, A. K., and Davis, S. H., "Steady Thermocapillary Flows in Two-Dimensional Slots," *Journal of Fluid Mechanics,* Vol. 121, 1982, pp. 163–186.

[10]Engelman, M. S., and Sani, R. L., "Finite Element Simulation of Incompressible Fluid Flows with a Free/Moving Surface," *Computational Techniques for Fluid Flow,* edited by C. Taylor, J. A. Johnson, and W. R. Smith, Pineridge, Swansea, Wales, UK, 1986, Chap. 3, pp. 47–74.

[11]Schwabe, D., private communication, 1989.

[12]Jackson, C. P., "The Effect of the Choice of the Reference Pressure Location in Numerical Modeling of Incompressible Flow," *International Journal for Numerical Methods in Fluids,* Vol. 4, 1984, pp. 147–158.